

Anisotropy of magnetic susceptibility in diamagnetic limestones reveals deflection of the strain field near the Dead Sea Fault, northern Israel



R. Issachar^{a,b,*}, T. Levi^b, S. Marco^a, R. Weinberger^{b,c}

^a Department of Geosciences, Tel Aviv University, Tel Aviv 6997801, Israel

^b Geological Survey of Israel, 30 Malkhe Israel Street, Jerusalem 95501, Israel

^c Department of Geological and Environmental Sciences, Ben-Gurion University of the Negev, Beer-Sheva 84105, Israel

ARTICLE INFO

Article history:

Received 28 January 2015

Received in revised form 9 June 2015

Accepted 12 June 2015

Available online 7 July 2015

Keywords:

Anisotropy of magnetic susceptibility

Dead Sea Fault

Deformation

Diamagnetism

Rock magnetism

ABSTRACT

To exploit the potential of anisotropy of magnetic susceptibility (AMS) as a tool to estimate the strain field around major faults, we measured the AMS of calcite-bearing diamagnetic rocks that crop out next to the Dead Sea Fault (DSF) in northern Israel. Through integrated magnetic and geochemical methods we found that the rocks are almost pure calcite rocks and therefore the magnetic fabric is primarily controlled by preferred crystallographic orientation (PCO) with the minimum principal AMS axes (k_3) parallel to calcite *c*-axes. We applied a separation procedure in several samples with high Fe content in order to calculate the AMS anisotropy parameters and compare them to pure diamagnetic rocks. AARM, thermo-susceptibility curves and IRM were used to characterize the magnetic phases. We found that for Fe content below 500 ppm the AMS is mostly controlled by the diamagnetic phase and showed that differences in the degree of anisotropy P' up to 3% ($P' = 1.005$ to 1.023) and in anisotropy difference Δk (up to $\sim 0.25 \times 10^{-6}$ SI) in diamagnetic rocks are related to differences of strain magnitudes. The spatial distribution of the magnetic fabrics indicates \sim N–S maximum shortening parallel to the strike of the Hula Western Border fault (HWBF), one of the main strands of the DSF in northern Israel. The anisotropy parameters suggest that the strain magnitudes increase eastward with the proximity to the HWBF. These results suggest that the strain field near the HWBF is locally deflected as a consequence of the DSF activity. In light of the “fault weakness” model and geological setting of the study area, we suggest that the area accommodates dominant transtension during the Pleistocene. The present study demonstrates the useful application of AMS measurements in “iron-free” limestones as recorders of the strain field near plate boundaries.

© 2015 Elsevier B.V. All rights reserved.

1. Introduction

Determining the strain field around plate-bounding faults is important for understanding the mechanism of fault activity at the upper crust and critical for assessing hazards due to fault reactivation (e.g., Nuchter and Ellis, 2011). Despite the importance of this determination, reconstructing the strain field around major faults obtained by analysis of kinematic indicators (e.g., fractures, striations, veins, folds) is usually hampered by the absence of these indicators or their complex interpretation.

The texture of calcite-bearing rocks is considered one of the most reliable strain-sensitive petrofabric indicators, because under tectonic loading the *c*-axes of calcite crystals are usually aligned parallel to the direction of maximum shortening (Bestmann et al., 2000; Borradaile and Jackson, 2010; de Wall et al., 2000; Rutter and Rusbridge, 1977; Rutter et al., 1994). This has been observed in laboratory experiments, when the *c*-axes of calcite crystals tend to align parallel to the direction of maximum shortening under loading (Hounslow, 2001; Kamb, 1959; McKenzie et al., 1996; Neumann, 1969; Patterson, 1973; Tullis and

Yund, 1982). In such cases, preferred crystallographic orientation (PCO) may develop in calcite-bearing rocks in association with a variety of crystal-plastic deformation mechanisms (Bishop, 1953; Bishop and Hill, 1951; Calnan and Clews, 1950, 1951; Evans et al., 2003; Hobbs et al., 1976). Several attempts have been made to estimate the PCO by measuring the anisotropy of magnetic susceptibility (AMS) of calcite-bearing rocks and correlate the AMS principal axes with strain axes (Almqvist et al., 2010; de Wall et al., 2000; Hamilton et al., 2004; Levi and Weinberger, 2011; Schmidt et al., 2006). This application of the AMS is complicated by the weak diamagnetic response of the carbonate rocks, and the possible overprint of paramagnetic and ferromagnetic phases. The advance in laboratory apparatuses enables accurate and reproducible measurement of diamagnetic AMS (Levi and Weinberger, 2011; e.g., Braun et al., 2015). To fully exploit the potential of this application the AMS has to primarily represent the diamagnetic phase. This is possible if the carbonate rock is almost purely diamagnetic, or if the diamagnetic phase could be separated from the paramagnetic and ferromagnetic phases (Borradaile and Jackson, 2010).

The active Dead Sea Fault (Transform) system accommodates \sim 105 km of the relative left-lateral motion between the Arabian and Africa (Sinai) plates since the early–middle Miocene (e.g., Garfunkel,

* Corresponding author.

E-mail address: ranissachar@gmail.com (R. Issachar).

1981). The long-term regional/remote strain field associated with the Dead Sea Fault (DSF) was determined based on meso-scale structures (Bartov et al., 1980; Eyal, 1996; Eyal and Reches, 1983). However, the local spatial and temporal variations of the strain field and its partitioning within the deformed blocks near the DSF are not well constrained. Insights into these variations are important in terms of reconstructing the tectonic evolution of the DSF and assessing its seismic hazard, and may be relevant in assessing other fault zones worldwide. In particular, the possibility that the trajectories of the stress/strain field have been deflected next to the DSF and other transforms has been suggested (Garfunkel, 1981; Zoback et al., 1987), but need further support from meso-scale kinematics. The lack of information on the DSF-related local strain is partly due to the absence of reliable kinematic indicators that have been developed next to the DSF.

The present study uses the AMS method in calcite-bearing limestones of the Eocene Bar-Kokhba Formation from outcrops near the DSF. This formation, one of the last pre-DSF widespread marine deposits, is characterized by low iron content (<400 ppm) and diamagnetic response and was previously studied by Levi and Weinberger (2011). Our main objectives are (1) to establish the AMS-strain relations in diamagnetic carbonate rocks, and (2) to analyze the strain field next to the DSF in northern Israel.

2. AMS in carbonate rocks and deformation

The magnetic susceptibility (k) is a physical property of a material that indicates its capacity to be magnetized (M) under an applied magnetic field (H). At low applied fields the magnetization is linear ($M_i = k_{ij}H_j$) and the susceptibility is field independent (Cullity, 1972). The AMS is described by three principal axial values k_1 , k_2 and k_3 , which correspond to the maximum, intermediate and minimum magnetic susceptibility magnitudes, respectively (e.g., Borradaile and Jackson, 2004). The AMS parameters that are used most frequently for describing the axial magnitude relationships are the mean susceptibility, $k_m = (k_1 + k_2 + k_3)/3$ (Nagata, 1961), the susceptibility difference $\Delta k = k_1 - k_3$ (Jelinek, 1981), the corrected anisotropy degree $P' = \exp\sqrt{2\sum(\ln k_i - \ln k_m)^2}$ ($i = 1$ to 3 , k_m is the mean susceptibility) (Jelinek, 1981), the magnetic lineation $L = k_1/k_2$ (Balsley and Buddington, 1960), the magnetic foliation ($F = k_2/k_3$) (Stacey et al., 1960), and the AMS shape parameter $T = 2 \ln(k_2/k_3)/\ln(k_1/k_3) - 1$ (Hrouda, 2004), measuring the range from prolate ($-1 < T < 0$) through neutral ($T = 0$) to oblate ($0 < T < 1$) ellipsoids (Jelinek, 1981). For diamagnetic rocks, the AMS parameters are calculated based on the absolute (unsigned) values of the principal susceptibility (Hrouda, 2004) and the AMS parameters are then $P' = \exp\sqrt{2\sum(\ln|k_i| - \ln|k_m|)^2}$ ($i = 3$ to 1); $L = |k_3|/|k_2|$; $F = |k_2|/|k_1|$; and $T = 2 \ln(|k_2|/|k_1|)/\ln(|k_3|/|k_1|) - 1$.

AMS axes show a fair to good correlation with the directions of the principal strain axes in different deformed rocks and geological settings (Almqvist et al., 2009; Borradaile, 1987, 1988, 1991; Borradaile and Henry, 1997; Borradaile and Jackson, 2004; Cogne and Perroud, 1988; Dietrich and Song, 1984; Hirt et al., 1988; Hrouda et al., 2009; Jayangondaperumal et al., 2010; Latta and Anastasio, 2007; Mamtani and Sengupta, 2009; Pares et al., 1999; Soto et al., 2007, 2009; Tarling and Hrouda, 1993). Several studies on calcite-bearing rocks show a good agreement between the orientations of the calcite c -axes and k_3 axes (e.g., Almqvist et al., 2011; Chadima et al., 2004; de Wall et al., 2000; Kligfield et al., 1982; Owens and Rutter, 1978; Siegesmund et al., 1995; Wenk et al., 1987). Generally, clustering of the k_3 axes parallel to the direction of maximum remote (tectonic) shortening in carbonate rocks (Borradaile and Hamilton, 2004; Hamilton et al., 2004 and references therein).

During compaction and lithification processes some of the c -axes could align with the lithostatic pressure, depending on the pressure magnitude (Hrouda, 2004). Hence, under depositional environment

associated with a dominant compaction process (e.g., Borradaile and Henry, 1997) the k_3 axis is vertical and parallel to the direction of maximum shortening ($k_3 \parallel c$ -axes), and k_1 and k_2 are parallel to bedding and form magnetic foliation. Under tectonic environment (shortening or extension regimes), the AMS axes are generally parallel to the principal strain directions ($X \geq Y \geq Z$), where X is the maximum elongation, Y is intermediate strain axis and Z is the maximum shortening. Consequently, $k_1 \parallel X$, $k_2 \parallel Y$, $k_3 \parallel Z$, and the AMS fabric is termed 'normal' ($k_3 \parallel c$ -axes) (e.g., Borradaile and Jackson, 2010).

Calcite single crystal is magnetically anisotropic, characterized by the corrected anisotropy degree, $P' = 1.113$ (Owens and Bamford, 1976), the susceptibility difference, $\Delta k = 1.10 \pm 0.01 \times 10^{-6}$ SI (Schmidt et al., 2006) and the anisotropy shape, $T = -1$ (Owens and Bamford, 1976). The AMS shape of pure calcite crystal at room temperature is perfectly prolate and it switches to oblate above Fe concentration of ~400 ppm (Schmidt et al., 2006; but note that according to their definition a pure calcite crystal is perfectly oblate using the U parameter). The AMS of the diamagnetic fraction in calcite-bearing rocks should be lower than the anisotropy of single crystals or deformed calcite-bearing rocks, because perfect alignments are rare, especially in sedimentary rocks (Hrouda, 2004 and references therein).

Limited success and no reliable correlation has been established between the magnitudes of the AMS axes of carbonated rocks and finite strain magnitudes (e.g., Borradaile and Jackson, 2010; Latta and Anastasio, 2007; Parés and Van der Pluijm, 2004; Tripathy et al., 2009). One major cause for this lack of success is the low susceptibility value of calcite ($k_m \approx -12.87 \times 10^{-6}$ SI (Nye, 1957; Owens and Rutter, 1978); $k_m \approx -12.09 \times 10^{-6}$ SI (Schmidt et al., 2006)), which is easily affected by Fe and Mn bearing minerals in the rock (Almqvist et al., 2010; Borradaile and Henry, 1997; Schmidt et al., 2006).

Several studies have shown a good correlation between the increase in anisotropy parameters and increase of strain magnitudes. Schmidt et al. (2009) show in a series of compaction experiments of synthetic calcite-muscovite samples that the susceptibility difference (Δk) is generally increases with strain magnitudes. Almqvist et al. (2009) find an agreement between the calculated Δk based on the PCO intensity and the measured Δk of the diamagnetic phase of limestones in the Morcles Nappe complex. Levi and Weinberger (2011) suggest based on AMS studies in calcite-bearing diamagnetic rocks, that the differences in Δk are related to differences in strain magnitudes.

3. Geological setting

The DSF system extends from the northern end of the Red Sea rift to the Taurus convergence zone in Turkey, passing through the Gulf of Elat-Aqaba, the Dead Sea rift in Israel, Lebanon and Syria. A host of stratigraphic, structural and geochronological evidence suggests ~105 km of left-lateral offset across the DSF (Freund et al., 1970; Garfunkel, 1981; Quennell, 1959). Eyal and Reches (1983) and Eyal (1996) interpreted middle Miocene to Recent NNW maximum horizontal shortening and ENE extension. This remote strain field has been associated with the sinistral displacement along the DSF and the opening of the Red Sea, and is attributed to the Dead Sea stress field.

Several pull-apart basins have developed along the DSF system (e.g., the Gulf of Elat-Aqaba, the Dead Sea, the Sea of Galilee, and the Hula Valley). The Rosh-Pinna area is located between the Sea of Galilee and the Hula basin (Fig. 1) west and near the southward continuation of the Hula Western Border Fault (HWBF), one of the main strands of the DSF in northern Israel (Freund et al., 1970; Sneh and Weinberger, 2014), where the mid-Eocene Bar-Kokhba Formation limestones are widely exposed. The beds dip gently southeastward with some local variations. The underlying early-Eocene Timrat Formation is exposed at the base of the Rosh-Pinna stream (Fig. 1). Between the HWBF and the Almagor Fault in the east (Fig. 1) an elevated area known as the Korazim block is exposed and extensively covered by Plio-Pleistocene basalts (Heimann and Ron, 1993; Rotstein and Bartov, 1989). Based on

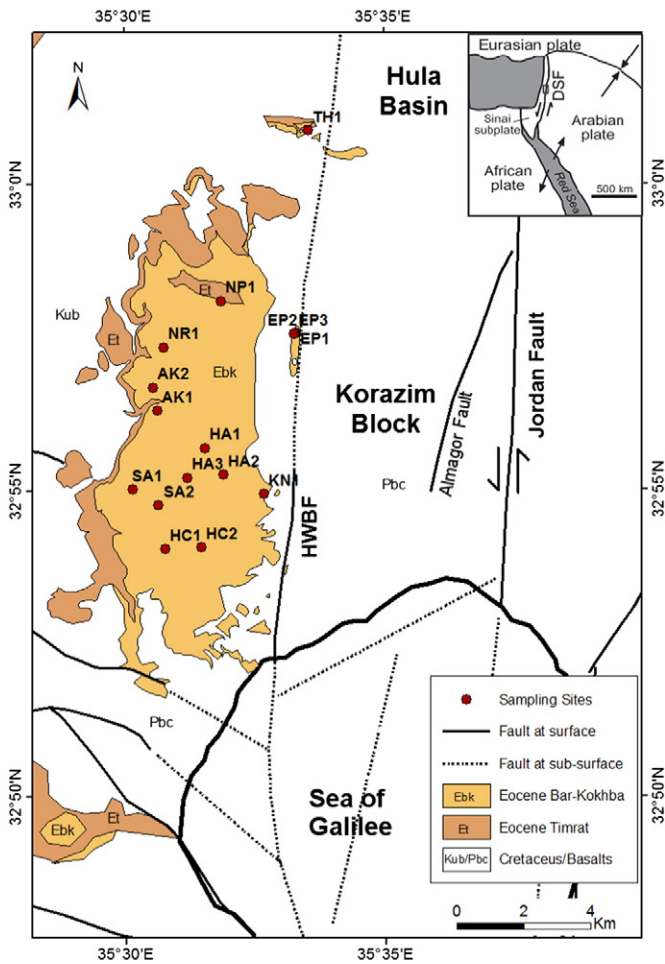


Fig. 1. Geological map of the study area and sampling sites. Names of faults are marked (Sneh and Weinberger, 2014). HWF—Hula Western Border Fault. The inset shows the plate tectonic configuration resulting in left-lateral motion across the DSF. Geological sections after Levitte, D. (2001), Sneh, A. and Weinberger, R. (2006), and Bogoch, R. and Sneh, A. (2008).

paleomagnetic measurements it was suggested that Korazim experienced counterclockwise block rotation not before 0.9 Ma (Heimann and Ron, 1993).

4. Sampling strategy and methods

4.1. Sampling strategy

In order to determine whether the magnetic fabrics near the DSF are a product of the remote strain field or the consequence of disturbances and deflection of the local strain field, three sites (EP1–EP3) were sampled several meters away from the southward continuation of the HWBF, two sites (KN1 and TH1) 1 km, four sites (NP1, HA1, HA2, HC2) ~3 km, and seven sites (SA1, SA2, HC1, AK1, AK2, HA3, NR1) ~3–5 km away from the HWBF (Fig. 1). A total of 212 samples were taken from the 16 sites within the Rosh-Pinna area.

4.2. Chemical and mineralogical composition

To determine the chemical composition and the bulk mineralogy of the carbonate rocks and to test the possible effect of Fe and Mn ions on the magnetic fabrics several laboratory and optical analyses were carried out at the Geological Survey of Israel. The chemical composition of 18 samples was analyzed by ICP-OES optima 3300 and trace element content of five samples was analyzed by ICP-MS Elan 6000. Powders

were side-packed into aluminum holders. Semi-quantitative composition was estimated by comparison with calibration curves and with the corresponding chemical data. The amount of insoluble residue was measured for each sample. The micro-scale chemistry and structures were analyzed by Scanning Electron Microscope (SEM) model FEI Quanta 450 equipped with an EDS detector. The bulk mineralogy of 10 samples was also analyzed by X-ray diffraction (XRD) using Philips PW1730/1710, and PW1830/3710, CuK α 1 Representative thin-sections were analyzed with an optical polarizing microscope for better understanding of the lithology and the sedimentary environments.

4.3. Magnetic fabrics

The tectonic significance of weak magnetic susceptibilities requires special consideration (Hamilton et al., 2004; Levi and Weinberger, 2011) in particular with AMS data of diamagnetic rocks such as the Bar-Kokhba limestone. The AMS was measured at low magnetic field of 300 A/m with a KLY-4S Kappabridge (AGICO Inc.) at the Geological Survey of Israel. The sensitivity of the Kappabridge is of the order of 1×10^{-8} SI, enabling measurements of mean susceptibility of about 1×10^{-6} SI. Representative measurements were repeated three times to ensure reproducibility. We considered only samples that passed the F-test for 95% confidence interval (>3.9 ; Jelinek, 1977), or samples in which the principal AMS axes are within the 95% confidence intervals of the site mean tensor. The AMS confidences were derived according to Jelinek's (1981) procedure. The magnitudes and directions of the AMS principal axes were calculated using the software package Anisoft 42. The AMS axes of the diamagnetic rocks are described by the signed values of susceptibility, namely, the minimum susceptibility (k_3) refers to the most negative susceptibility value (Hrouda, 2004). In addition, the AMS parameters (P , T , L and F) are calculated based on the absolute (unsigned) values of the principal susceptibility, implying that the largest absolute magnitude is the maximum susceptibility (Hrouda, 2004).

The Anisotropy of Anhyseretic Remanent Magnetization (AARM) (Jackson, 1991; Jackson and Tauxe, 1991) of six selected samples from site SA1 was measured in order to test the possible contribution of the ferromagnetic phase to the bulk magnetic fabric of site SA1. The AARM was measured at the Geological Survey of Israel, with AF demagnetizer/magnetizer LDA-3/AMU-1 and a JR-6 spinner magnetometer (AGICO Inc.). First, AF demagnetization curve was measured for representative samples in order to determine the appropriate AC field. Next the remanent magnetization was imparted in six pairs of antiparallel directions with a DC field of 500 μ T and AC field of 50 mT. The AARM orientations and parameters were calculated using the *Arem2W* software package.

4.4. Rock magnetism

The Isothermal Remanent Magnetization (IRM) (Fuller et al., 1988; Stockhausen, 1998) was measured in order to characterize the ferromagnetic minerals involved in the carbonate rocks of site SA1. The magnetization was measured using a shielded three axes 2G 750R SRM cryogenic magnetometer, with integrated AF coils, at the Institute of Earth Sciences, the Hebrew University of Jerusalem. Each sample was subjected to a stepwise demagnetization with an increasing intensity starting at 5 mT and going up to 90 mT. Next the samples were exposed to a high pulse field using the ASC model IM10-30 Impulse Magnetizer, starting with a field of 25 mT up to 200 mT with increments of 25 mT, then steps of 50 mT up to 400 mT, and steps of 100 mT up to 1600 mT. After each step, the IRM was measured using the magnetometer.

The contribution of the ferromagnetic minerals was also assessed by temperature-dependence susceptibility measurements ($k-T$) at the Geological Survey of Israel, combining the KLY-4S kappabridge with CS-L (low temperature cryostat apparatus between -195 and 0 °C) and CS-3 furnace (temperature range between ~ 25 and 700 °C) (AGICO Inc.).

4.5. AMS separation procedure

Various of experimental techniques have been developed using the difference in the physical properties of different magnetic phases in order to identify the sub-fabrics of the AMS (Martin-Hernandez and Ferre, 2007 and references therein). In this study we designed a separation procedure using the mathematical properties of the AMS tensor in order to separate the pure calcite diamagnetic contribution from the bulk AMS fabric. The separation procedure helps to calculate the AMS parameters of the separated magnetic fabrics and further to compare them to AMS parameters of pure diamagnetic rocks. We choose site SA1 as a case study for applying the separation method. In this site iron rich second-phase material fill small cracks, which are distinctive from the bulk rock. This material is associated with young morphological processes of chemical alteration. Based on rock magnetism and chemical analysis (see Section 6.2), this site represents a case in which the AMS is composed mainly by two sub-fabrics.

The total susceptibility tensor of a specimen (k_t) is described as the sum of the ferromagnetic k_f , paramagnetic k_p , and diamagnetic k_d susceptibility tensors (Henry and Daly, 1983; Hrouda et al., 2000):

$$k_t = c_f k_f + c_p k_p + c_d k_d \quad (1.1)$$

and

$$c_f + c_p + c_d = 1 \quad (1.2)$$

where c_f , c_p and c_d are the respective percentages of the susceptibility tensors (Hrouda et al., 2000).

In general, the susceptibility tensor (k) can be constructed from the product of the normalized tensor (\hat{k}) and the mean susceptibility (k_m), which is also known as a norming factor (Jelinek, 1977):

$$k = k_m \cdot \hat{k} \quad (1.3)$$

Consider a rock consisting of two dominant magnetic phases—diamagnetic marked with sub index d and another phase, paramagnetic or ferromagnetic, marked with sub index α . Rewriting Eq. (1.1) for the two phases in that form:

$$k_{m_t} \cdot \hat{k}_t = c_\alpha k_{m_\alpha} \cdot \hat{k}_\alpha + c_d k_{m_d} \cdot \hat{k}_d \quad (1.4)$$

In this case the diamagnetic phase can be estimated using the following expression:

$$k_{m_d} \cdot \hat{k}_d = \frac{1}{1-c_\alpha} k_{m_t} \cdot \hat{k}_t - \frac{c_\alpha}{1-c_\alpha} k_{m_\alpha} \cdot \hat{k}_\alpha \quad (1.5)$$

Since the susceptibility tensors are normalized, the total mean susceptibility can be written as:

$$k_{m_t} \cong c_\alpha k_{m_\alpha} + c_d k_{m_d} \quad (1.6)$$

and using Eq. (1.2):

$$k_{m_t} \cong (k_{m_\alpha} - k_{m_d}) c_\alpha + k_{m_d} \quad (1.7)$$

Generally, the mean susceptibility values of the paramagnetic/ferromagnetic minerals are much greater than the value of the diamagnetic mean susceptibility, $k_{m_\alpha} \gg k_{m_d}$, and hence:

$$k_{m_t} \cong k_{m_\alpha} c_\alpha + k_{m_d} \quad (1.8)$$

If c_α , k_{m_α} and \hat{k}_α can be estimated then it is possible to separate the diamagnetic AMS sub-fabric of rocks consisting two dominant magnetic phases using Eqs. (1.5) and (1.8).

Eq. (1.8) predicts a linear correlation between k_{m_t} and c_α for the element carrying the para/ferromagnetic phase, where the slope represents k_{m_α} and the intersection with the k_{m_t} axis represents k_{m_d} . A chemical composition analysis can be used to estimate the respective percentages (c_α) of the elements involved in the rock (Schmidt et al., 2006). By performing such an analysis for a group of specimens in site SA1 the relations between the specimens' bulk susceptibilities (k_{m_t}) and the respective amounts of certain element (c_α) can be examined.

5. Results

5.1. Petrography, mineralogy and geochemistry

Optical microscopy images of selected samples indicate that the rock includes nummulites and fragments of shells (Appendix Fig. A.1). SEM and EDS analysis indicate that the rock is made of almost pure calcite crystals, which are characterized by grain size ranging between few to couple of dozens of microns. XRD results of selected samples confirm that the Bar-Kokhba limestones consists of calcite as the most dominant (>95%) mineral.

The average contents of Fe and Mn of nine representative samples are <300 and >10 ppm, respectively (Table 1). The average contents of Al, Fe and Mg of the 11 paramagnetic samples of site SA1 are 1272, 1135 and 1445 ppm, respectively (Table 1).

5.2. Rock magnetism

The mean susceptibilities k_m indicate that the majority of the samples are diamagnetic with some weakly positive values indicating a paramagnetic and/or ferromagnetic content (Fig. 2; Table 2). The k_m values of samples from the Bar-Kokhba limestones fall in a narrow range between -8 and -12×10^{-6} SI with an average of $-10.57 \pm 1.76 \times 10^{-6}$ SI (excluding SA1 site). This value is very close to the value of a single calcite crystal (Section 2; Nye, 1957; Owens and Rutter, 1978; Schmidt et al., 2006).

High and low temperature curves of representative sample from NP1 site (Appendix Fig. B.1a) show almost temperature independency above -150 °C, corresponding to the diamagnetic characteristic of the sample. The heating curve of sample from SA1 site decreases between 320 and 700 °C, whereas the susceptibility decreases from 130×10^{-6} SI to 20×10^{-6} SI (Appendix Fig. B.1b). This may suggest the existence of ferromagnetic minerals, maybe even iron sulfides as its typical Curie

Table 1

Chemical content of selected samples. The results are in ppm.

Site name	Si	Al	Mg	Fe	Mn
EP3	<1000	<200	1000	<50	<10
KN1	<1000	4000	2000	70	<10
NP1	2000	500	2700	300	–
HC1	<1000	400	1400	≤50	<10
HA3	<1000	≤200	1200	≤50	≤10
NR1	<1000	2400	2000	100	<10
SA2	≤1000	300	1300	<200	–
SA1-1	3000	2000	1200	1100	–
SA1-2	3000	1500	5000	1600	–
SA1-6	≤1000	700	1200	400	–
SA1-7	<1000	1000	1000	320	–
SA1-8	5000	2500	1000	1300	–
SA1-10	8000	3800	1500	5800	–
SA1-11	≤1000	400	800	300	–
SA1-12	<1000	1500	800	800	–
SA1-13	<1000	200	800	500	–
SA1-14	1000	<100	2000	175	–
SA1-15	≤1000	300	600	200	–

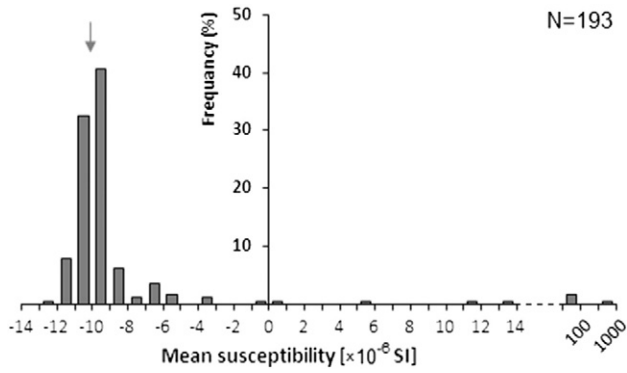


Fig. 2. Frequencies of the mean-susceptibilities (k_m) of all measured samples ($N = 193$). Arrow marks the histogram pick of the diamagnetic phase.

temperature is around $\sim 320^\circ\text{C}$ (Hunt et al., 1995). The cooling curve shows a large increase up to $\sim 380^\circ\text{C}$, suggesting the creation of new magnetic minerals during cooling.

The IRM of sample from SA1 site indicates the presence of low coercivity minerals that attain saturation just below 200 mT (Appendix Fig. C.1), typical of MD magnetite grains (Borradaile and Jackson, 2004; Mullins, 1977). After 200 mT, the curve continues moderately to increase, indicating the presence of high coercivity minerals.

5.3. AMS fabrics

Fig. 3 shows the projections of the AMS principal axes and their 95% confidence ellipses. The magnetic fabrics are divided into three main types based on the inclination of k_3 axes. In Type A, k_3 axes are sub-vertical, between 90° and 60° , in Type B between 60° and 30° and in Type C between 30° and 0° . These types are further divided into sub-types based on the orientation of k_1 and k_2 axes. In Type A1, k_1 and k_2 axes form a sub-horizontal magnetic foliation (SA1 site), while in Type A2, k_1 and k_2 axes are well-grouped. In Type B1, k_1 and k_2 axes form a sub-horizontal magnetic foliation (HA3 and EP1 sites), while in Type B2, k_1 and k_2 axes are well-grouped (AK2 and SA2 sites). In Type C1, k_1 and k_2 axes form a sub-horizontal magnetic foliation (HC1, NR1, NP1 and TH1 sites), while in Type C2, k_1 and k_2 axes are well-grouped

(EP3, HA1, HA2 and KN1 sites). Three sites (AK1, HC2 and EP2 sites) show an isotropic fabric and were excluded from a further analysis.

Fig. 4a shows the declinations and inclinations of the AMS principal axes of samples that have negative susceptibility values. The k_3 axes are characterized by clustered declinations trending to $\sim\text{N-S}$ with sub-horizontal inclinations. The k_2 axes are characterized by dispersed declinations and inclinations between 20° and 70° . The k_1 axes are characterized by clustered declinations trending to $\sim\text{E-W}$, with sub-horizontal inclinations. Fig. 4b shows the declination of Type C samples (i.e., k_3 inclination between 0° and 30°), excluding TH1 site. This site is situated in the northernmost part of the study area and shows orthogonal (E-W) k_3 directions.

The anisotropy parameter Δk varies between 0.05 and 0.29×10^{-6} SI (average of $\sim 0.13 \times 10^{-6}$ SI) (Table 2). These values are one order of magnitude lower than the published values of a single pure calcite crystal (Owens and Bamford, 1976; Schmidt et al., 2006). Fig. 5 shows the shape parameter (T) versus the anisotropy degree parameter (P') for all diamagnetic samples. For $P' > 1.02$ (about 5% from the samples), the AMS shape shows a possible tendency toward a prolate ellipsoid, which might be associated with a higher degree of c -axes alignment in the rock (Borradaile and Jackson, 2010). The Fe content is lower than 300 ppm in the diamagnetic samples, with a median value of 70 ppm. The anisotropy parameters (P' and Δk) show no dependency on Fe content or k_m (Appendix Fig. D.1). For example P' varies between ~ 1.005 and 1.025 for samples with Fe content of ~ 50 ppm (Appendix Fig. D.1).

5.4. The separated magnetic fabric

The k_m values of SA1 site range between -10 and 25×10^{-6} SI with one sample as an outlier at 109×10^{-6} SI. The AARM of six samples from SA1 show inconsistently oriented axes (Fig. 6a).

The AMS fabric indicates a mixture of two different fabrics (Type A1 and Type C1) in accordance with k_m values (Fig. 6). The Type A1 fabric is obtained for samples with $k_m > -1.53 \times 10^{-6}$ SI (Fig. 6b) while the Type C1 fabric is obtained for samples with $k_m < -4.90 \times 10^{-6}$ SI (Fig. 6c). The former represent the young weathered material. A positive relation between Fe contents and k_m is found (Fig. 7a) and used for separating the diamagnetic fabric. Next, km_d and km_α were estimated using Eq. (1.8) (see Section 4.5) by applying a linear regression of k_m versus Fe content (Fig. 7a). The regression yields $km_d = -12.78 \times 10^{-6}$ SI, which is close to the value a single calcite crystal (Schmidt et al., 2006), and $km_\alpha = 34,858 \times 10^{-6}$ SI. This value of km_α suggesting a

Table 2
Low-field AMS parameters. The anisotropy parameters are the average parameters for the sites.

Site name	Stratigraphic unit	Sample size (N)	Mean susceptibility k_m [10^{-6} SI]	Corrected anisotropy degree (P')	Susceptibility difference Δk [10^{-6} SI]	Shape parameter (T)	Magnetic foliation (F)	Magnetic lineation (L)
EP1	Bar-Kokhba	4	-10.06	1.023	0.229	-0.538	1.005	1.017
EP3	Bar-Kokhba	13	-12.52	1.013	0.160	0.137	1.007	1.005
KN1	Bar-Kokhba	16	-11.31	1.009	0.097	0.050	1.002	1.004
TH1	Bar-Kokhba	12	-9.38	1.009	0.076	-0.148	1.004	1.005
HA1	Bar-Kokhba	11	-11.07	1.011	0.110	-0.210	1.005	1.006
HA2	Bar-Kokhba	11	-11.03	1.008	0.089	-0.051	1.004	1.004
HA3	Bar-Kokhba	17	-11.50	1.007	0.073	-0.101	1.003	1.004
HC1	Bar-Kokhba	7	-8.21	1.028	0.225	-0.383	1.007	1.020
SA2	Bar-Kokhba	19	-11.02	1.005	0.057	0.002	1.003	1.002
AK2	Bar-Kokhba	17	-11.81	1.009	0.096	-0.288	1.003	1.006
NR1	Bar-Kokhba	15	-11.22	1.012	0.130	-0.277	1.004	1.007
NP1	Bar-Kokhba	9	-11.72	1.006	0.064	-0.035	1.003	1.003
*AK1	Bar-Kokhba	9	-9.80	1.011	0.095	-0.106	1.004	1.006
*HC2	Bar-Kokhba	18	-9.98	1.006	0.051	0.116	1.003	1.002
*EP2	Bar-Kokhba	15	-8.90	1.059	0.210	-0.225	1.014	1.039
*SA1	Bar-Kokhba	19	5.71	1.036	0.278	0.036	1.016	1.019

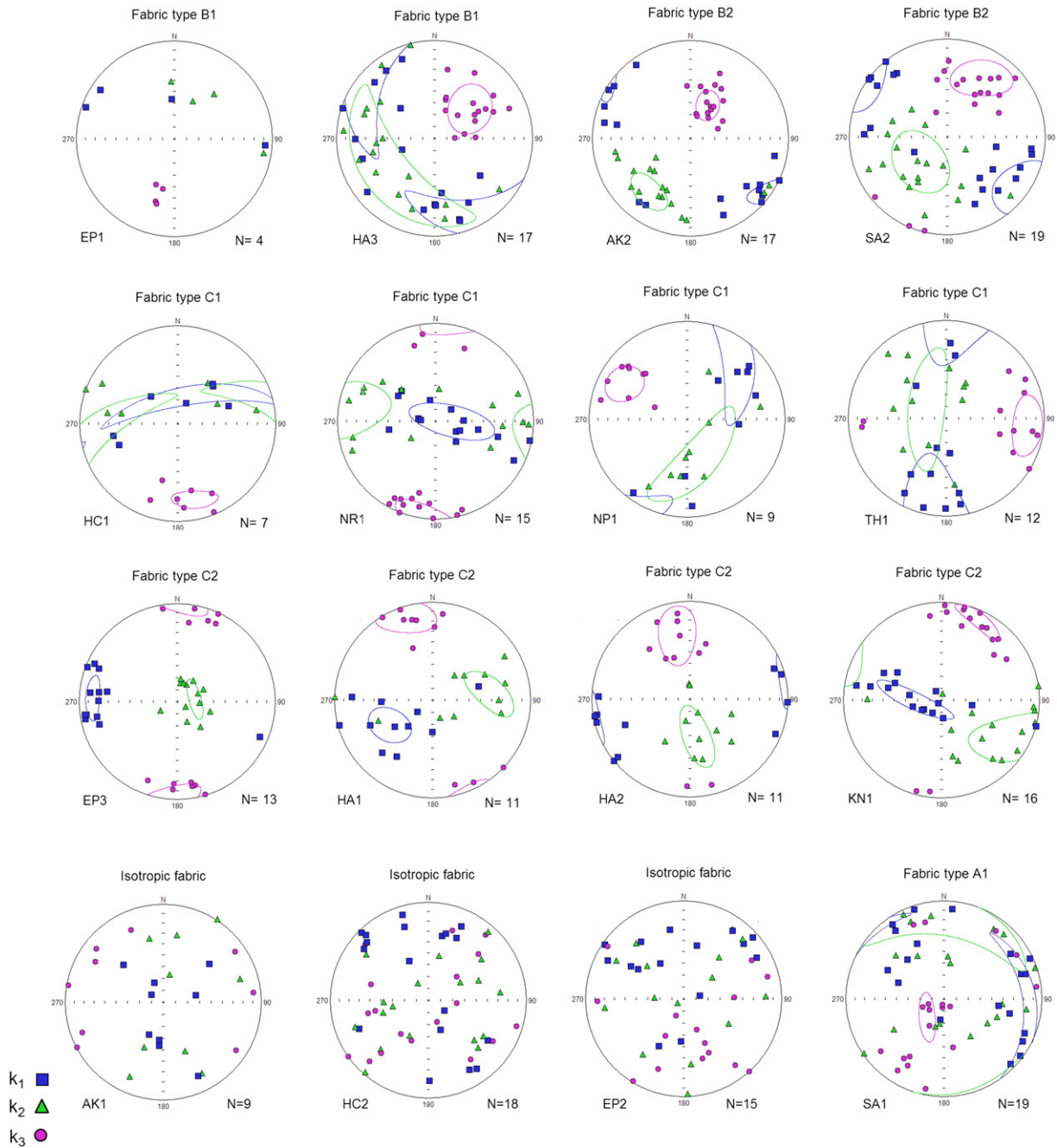


Fig. 3. AMS fabrics of the Bar-Kokhba limestone from the Rosh-Pinna area. Lower-hemisphere, equal-area projection of AMS principal axis and their 95% confidence ellipses. The k_1 , k_2 and k_3 axes are marked by solid squares (blue), triangles (green), and circles (purple), respectively.

mixture of paramagnetic and ferromagnetic iron-bearing minerals (Hunt et al., 1995).

To separate the diamagnetic sub fabric of SA1 site we solved Eq. (1.5) for all samples ($N = 19$). Note that k_{m_d} and k_{m_α} are similar for all the samples but c_α varies. These quantities derived from the linear regression described above (Fig. 7a). In addition, for \hat{k}_α we used the normalized tensor of the highest susceptibility sample in the site (SA1-10) for all samples. The separated diamagnetic sub-fabric shows characteristics of Type C2 fabric (Fig. 6d). The AMS parameters of the separated diamagnetic fabric are presented in Table 3. The P' values of 17 samples vary between 1.007 and 1.02, where two samples have $P' = \sim 1.045$. The T values are also varied and range between -0.7 and 0.8 .

6. Discussion

6.1. General

The present results were obtained after repeated measurements, especially for those samples that had negative susceptibilities. All measurements were reproducible and, hence, can be considered accurate albeit their low susceptibility values. The Bar-Kokhba limestones from the Rosh-Pinna area are calcite-bearing rocks containing extremely low amounts of Fe and Mn, less than 300 and 10 ppm, respectively (Table 1). The XRD results indicate that the Bar-Kokhba rocks consist of more than 95% calcite crystals. These and the bulk susceptibilities of

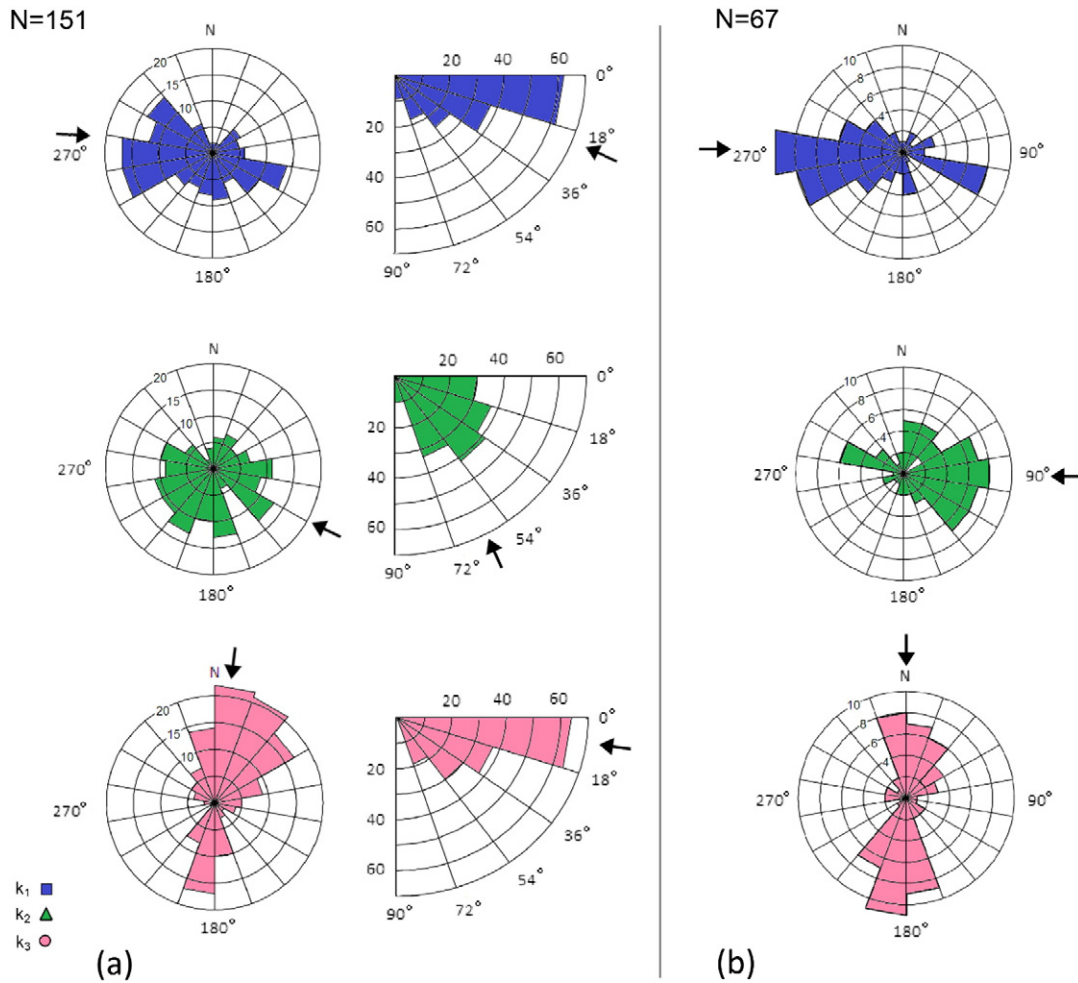


Fig. 4. Rose diagrams of AMS principal axes: (a) inclinations and declinations of all samples, excluded the isotropic sites and SA1 site (Fig. 3) and (b) declinations of magnetic fabrics Type C (k_3 inclination $<30^\circ$), excluded TH1 site. Arrows mark the average directions.

$k_m = -10.67 \pm 1.69 \times 10^{-6}$ SI indicate that the AMS is exclusively controlled by calcite crystals and, hence, the alignment of the AMS axes can be further discussed with relation to strain. The orientation of k_3 axes indicates the arrangement of calcite c -axes, which are aligned parallel to the maximum shortening axis (Borradaile and Hamilton, 2004; Hamilton et al., 2004 and references therein).

The AMS of diamagnetic rocks may depend on iron-bearing impurities (Almqvist et al., 2010; Borradaile et al., 2010; Hamilton et al., 2004; Schmidt et al., 2009) and substitution of Fe and Mn ions in the calcite lattices (Schmidt et al., 2007). In this case, the correlation between anisotropy parameters (P' and Δk) and strain magnitudes is questionable (Borradaile and Henry, 1997). In this study P' and Δk values of the Bar-Kokhba rocks ranges between 1.005 and 1.038 and between 0.05 and 0.3×10^{-6} SI, respectively (Table 2). Yet, the present P' and Δk values show no correlation to Fe content or k_m (Appendix Fig. D.1), suggesting that the anisotropy parameters are not controlled by impurities or second-phase minerals. Furthermore, the separation procedure shows that in the separated diamagnetic phase there are still significant variations in P' values between 1.007 and 1.045 (Table 3). This implies that these variations are related mainly to the alignment of the calcite c -axes.

Changes in the magnitude of the anisotropy parameters of carbonate rocks were attributed to strain intensity rather than to Fe impurities (Owens and Rutter, 1978; e.g., Almqvist et al., 2009; Schmidt et al.,

2009; Levi and Weinberger, 2011). Deformation experiments on Carrara marble (Owens and Rutter, 1978) showed that Δk attains saturation after $\sim 40\%$ shortening and reduces to half after $\sim 15\%$ shortening. Schmidt et al.'s (2009) experiments show that Δk in pure-calcite rocks generally increases up to $\sim 0.2 \times 10^{-6}$ SI when the uniaxial stress reaches to ~ 100 MPa. Almqvist et al. (2009) reported that in carbonate mylonites from the Morcles Nappes in Switzerland, increase of anisotropy degree is related to increase of strain magnitudes. Levi and Weinberger (2011) proposed that different values of Δk (up to $\sim 0.2 \times 10^{-6}$ SI) in the Bar-Kokhba rocks are related to differences in strain magnitudes. Based on the present results and the aforementioned studies, we suggest that variations in P' and Δk of the Bar-Kokhba rocks are related to the strain magnitudes that accumulated in the rocks during geological history (see below).

6.2. Separating the diamagnetic phase in carbonate rocks

By applying the separation procedure we are able to determine whether differences in AMS parameters are a result of chemical contamination or variations in the accumulated strain magnitudes. Moreover, the separation procedure suggests that the value of >500 ppm Fe content masks the diamagnetic fabric.

Based on rock magnetic measurements and chemical analysis it is suggested that the total AMS fabric of SA1 site is composed only of

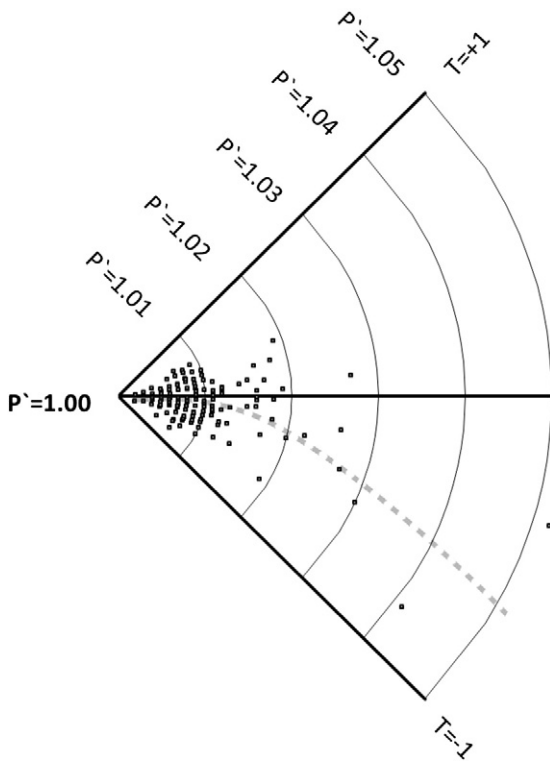


Fig. 5. Corrected anisotropy degree (P') and shape parameter (T). AMS data of Bar-Kokhba limestones, presented on a $\pi/4$ segment polar plot. P' is represented by the radius and T by the arc length (Borradaile and Jackson, 2004). T goes to -1 with growth of P' implying the development of PCO of calcite.

diamagnetic and paramagnetic sub-fabrics. First, we show correlation between k_m and Fe content (Fig. 7a) on one hand, and between k_m and the AMS fabric (Fig. 6b, c) on the other hand. This suggests that the AMS fabric of samples with high susceptibility values (Fig. 6b) is associated with iron-bearing minerals. Second, the inconsistently oriented AARM fabric suggests that the total AMS fabric is not influenced by ferromagnetic minerals. Therefore, we associate the paramagnetic sub-fabric with iron-bearing minerals even though a very small fraction of ferromagnetic minerals might exist as indicated by the linear regression of k_m versus Fe content (Fig. 7a) and by the IRM (Appendix Fig. C.1). We

note that the paramagnetic sub-fabric, which is represented by the high susceptibility samples (Fig. 6b), is characterized by Type A1 fabric of depositional origin. This fabric is related to iron-bearing minerals which evolved due to chemical alteration during a late weathering process. The diamagnetic sub-fabric on the other hand, is characterized by Type C2 fabric (Fig. 6c), which is associated with tectonic environment. Fig. 8 shows the relations between the inclinations of k_3 from site SA1 versus the Fe content of the associated samples. The results suggest that for Fe content >500 ppm, the k_3 inclinations $>60^\circ$ belong to the paramagnetic sub-fabric namely (Type A). For Fe content <500 ppm, the k_3 inclinations $<30^\circ$ belong to the diamagnetic sub-fabric (Type C). This analysis suggests that above a Fe threshold value of ~ 500 ppm, the diamagnetic fabric is masked and the paramagnetic phase controls the bulk AMS fabric.

6.3. AMS fabrics

The majority of the obtained magnetic fabrics are classified as Types C and B. These types, also known as “tectonic fabric” or “deformation fabric”, obliterates previous fabric due to increased shortening (Borradaile, 1988; Borradaile and Henry, 1997). Nine magnetic fabrics were classified as Type C, four as Type B and three are isotropic indicating that $\sim 80\%$ are tectonic fabrics. This finding is in agreement with the results of Levi and Weinberger (2011), who show that $\sim 85\%$ of the magnetic fabrics in Metulla block are distinctly “tectonic fabrics”.

The magnetic fabrics characteristics of the Rosh-Pinna area depend on their distance from the HWBF. Site EP3, located at the HWBF (Fig. 9), shows Type C2 fabric, which is characterized by the tightest grouping of the AMS axes and high anisotropy ($P' = 1.013$; $\Delta k = 0.16$). The k_3 axes are horizontal and oriented N–S. Sites HA1, HA2 and KN1, located ~ 3 km from the HWBF show also Type C2 fabrics that are relatively weakly grouped and have lower degree of anisotropy ($P' = 1.011$ to 1.008 ; $\Delta k = 0.11$ to 0.09) than EP3 site. The k_3 axes are horizontal and oriented N–S. The magnetic fabrics of sites, AK2, HA3, SA2 and HC1 that located ~ 6 km from the HWBF, show magnetic fabrics of types B2, B1 and C1, respectively. In these fabrics the magnetic foliations of k_1 and k_2 axes are more prominent, laying on planes that strike NW–SE. The k_3 axes of these magnetic fabrics are oriented \sim NE and dip $\sim 40^\circ$, possibly implying a composite of depositional and tectonic fabrics. The anisotropy values of these magnetic fabrics (AK2, HA3, SA2) are slightly lower ($P' = 1.009$ to 1.005 ; $\Delta k = 0.09$ to 0.06). HC1 site is an exceptional because it is characterized by a relatively very high anisotropy ($P' = 1.028$, $\Delta k = 0.225$), possibly due to the presence of paramagnetic minerals

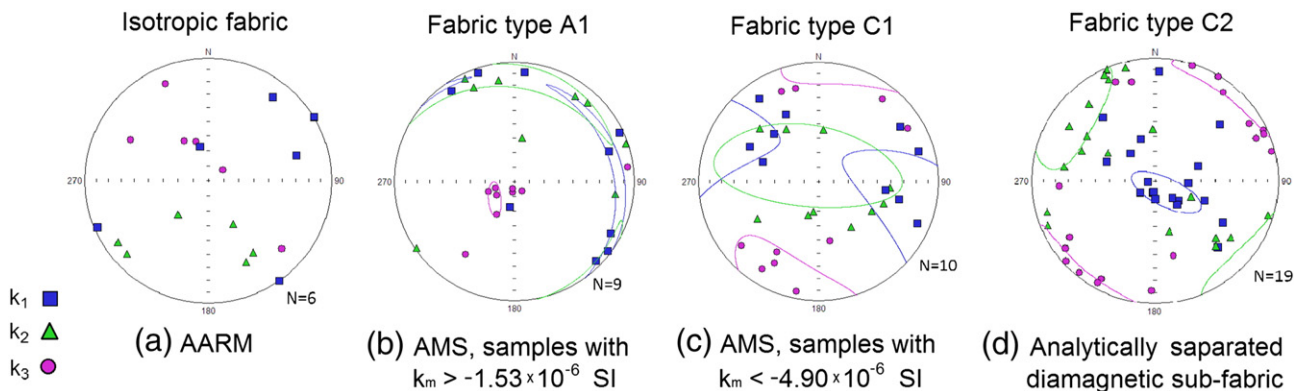


Fig. 6. Lower-hemisphere, equal-area projection and the 95% confidence ellipses of samples from SA1 site: (a) AARM fabric of selected samples, showing inconsistently oriented axes. (b) AMS fabric of samples with mean susceptibilities larger than -1.53×10^{-6} SI. (c) AMS fabric of samples with mean-susceptibilities lower than -4.90×10^{-6} SI. (d) Results of the separation procedure showing the AMS fabric of the diamagnetic phase.

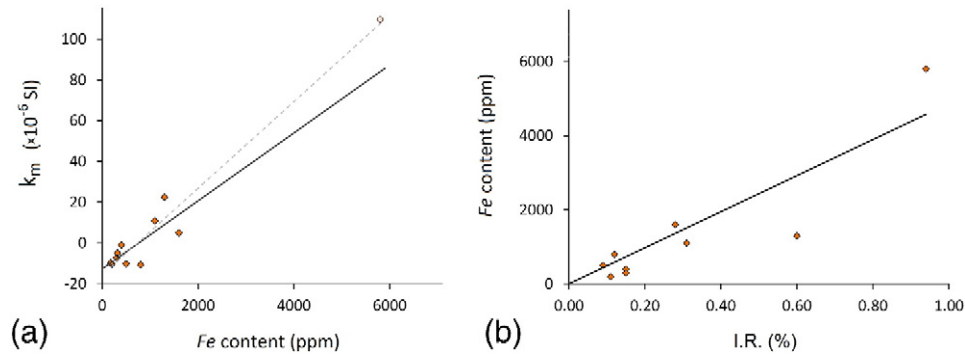


Fig. 7. (a) Mean susceptibility (k_m) versus Fe content in SA1 site. The linear regression marked with solid line considers only values that marked with filled diamonds. The regression coefficient is $R^2 = 0.57$. (b) Fe content versus insoluble residue (I.R.%). The high correlation ($R^2 = 0.80$) suggests that most of the Fe content is associated with young weathered material (see text for details).

Table 3
AMS parameters of the diamagnetic phase of SA1 site, results of separation procedure.

Sample No.	Mean susceptibility k_m [10^{-6} SI]	Corrected anisotropy degree (P')	Susceptibility difference Δk [10^{-6} SI]	Shape parameter (T)	Magnetic foliation (F)	Magnetic lineation (L)
1.	-12.79	1.020	0.253	0.316	1.013	1.007
2.	-12.78	1.013	0.165	0.030	1.007	1.006
3.	-12.78	1.009	0.115	-0.636	1.002	1.007
4.	-12.79	1.043	0.537	0.580	1.034	1.009
5.	-12.79	1.046	0.574	-0.295	1.016	1.029
6.	-12.78	1.010	0.127	0.417	1.007	1.003
7.	-12.79	1.020	0.253	0.421	1.014	1.006
8.	-12.82	1.016	0.203	0.802	1.014	1.002
9.	-12.79	1.019	0.241	0.364	1.013	1.006
10.	-12.78	1.015	0.195	0.253	1.010	1.006
11.	-12.78	1.007	0.089	-0.442	1.002	1.005
12.	-12.78	1.013	0.165	-0.150	1.006	1.007
13.	-12.78	1.014	0.178	-0.618	1.003	1.011
14.	-12.78	1.010	0.127	-0.334	1.003	1.007
15.	-12.78	1.014	0.178	-0.703	1.002	1.012
16.	-12.78	1.007	0.089	0.110	1.004	1.003
17.	-12.78	1.008	0.102	0.019	1.004	1.004
18.	-12.78	1.008	0.106	-0.383	1.003	1.006
19.	-12.78	1.016	0.203	-0.512	1.004	1.012
Ave.*	-12.78	1.016	0.205	-0.040	1.008	1.008
Mean**	-12.78	1.012	0.153	0.144	1.007	1.005

* Averaged parameters.
** Mean tensor parameters.

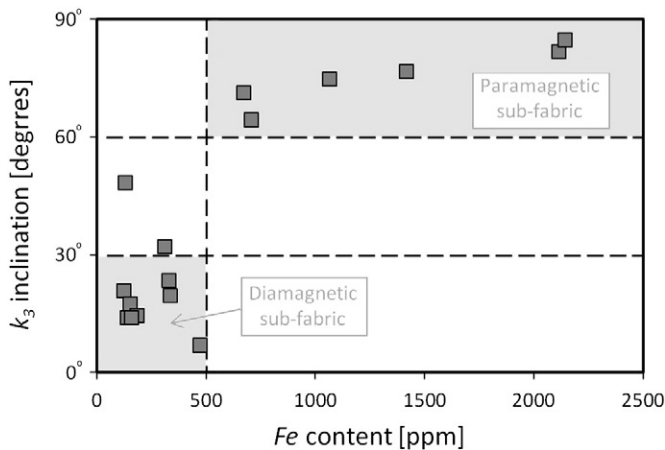


Fig. 8. k_3 inclination versus Fe content of samples from SA1 site. The Fe contents in ppm are estimated from the linear regression (Fig. 7a). The fields are marked with gray; the diamagnetic sub-fabric (Fe < 500 ppm and $0^\circ < k_3 < 30^\circ$) and the paramagnetic sub-fabric (Fe > 500 ppm and $60^\circ < k_3 < 90^\circ$).

as indicated by the bulk susceptibilities. In the northern parts of the Rosh-Pinna area, the magnetic fabrics of TH1 and NP1 sites are of Type C1. The foliation plane is vertical, striking N–S, and the k_3 axes are oriented E–W to WNW–ESE. Site NR1 also shows Type C1 fabric with N–S oriented k_3 axes, despite its distance (~6 km) from the HWBF.

6.4. Strain field next to the DSF in the Rosh-Pinna area

The tectonic fabrics obtained in this study suggest that the deformation in the Rosh-Pinna area gradually varies eastward with slightly increase of the strain magnitudes toward the HWBF. The statistical analysis of the k_3 and k_1 axes in this area (apart from two sites at the northernmost part) indicates that the directions of maximum shortening (parallel to k_3) is ~N–S and that of maximum elongation (parallel to k_1) is ~W–E (Figs. 4 and 9). Hence, the remote NNW–SSE maximum horizontal shortening (Eyal, 1996) deflects toward the HWBF, showing local ~N–S maximum shortening near this fault.

Similar to the present approach, Levi and Weinberger (2011) considered the magnetic fabrics of the Eocene Bar-Kokhba and

Upper Miocene Kefar–Giladi formations next to the northward continuation of the HWBF in the Metulla block. They obtained tectonic fabrics that dominantly indicate ~W–E maximum shortening in relation to strain partitioning along the DSF in northern Israel during the Pleistocene (Weinberger et al., 2009). Unlike the findings in the Metulla block, indication for ~W–E maximum shortening was found only in the northernmost part of Rosh-Pinna area (sites TH1 and NP1), while in the other parts ~N–S shortening directions are dominant. Hence, the northernmost part of the Rosh Pinna area shows affinity to the deformation in the Metulla block. If the ~W–E shortening directions in the Metulla block and the ~N–S shortening directions in the Rosh Pinna area are coeval, then locally the maximum shortening directions have been switched by ~90° between these zones during the Pleistocene.

In what follows, we show that this AMS-based strain field in the Rosh-Pinna area is local and closely related to the DSF. The revealed

~N–S maximum shortening direction is parallel to the strike of the HWBF and the general trend of the DSF in northern Israel (Fig. 9). This direction deviates by ~15° from the remote NNW–SSE maximum shortening direction since the middle Miocene (the “Dead Sea Strain field” of Eyal and Reches, 1983; Eyal, 1996). Notably, a local horizontal maximum shortening of ~N–S was inferred from stylolites in the Eocene rocks of the Rosh Pinna area (Eyal, 1996; Ron and Eyal, 1985). Based on this direction and directions inferred from other meso-structures, Ron and Eyal (1985) reconstructed a trajectory map of the maximum horizontal compression in northern Israel and showed that locally it deflects and becomes parallel to the ~N–S strike of the DSF. Arkin (1996) studied fractures in the Rosh Pinna area and in particular a set of ~N–S striking fractures, which are undulating, open-mode fissures associated with karstic features such as solution rills, calcite precipitates and soil staining. Arkin et al. (2004 and personal communication, 2014) attributed the

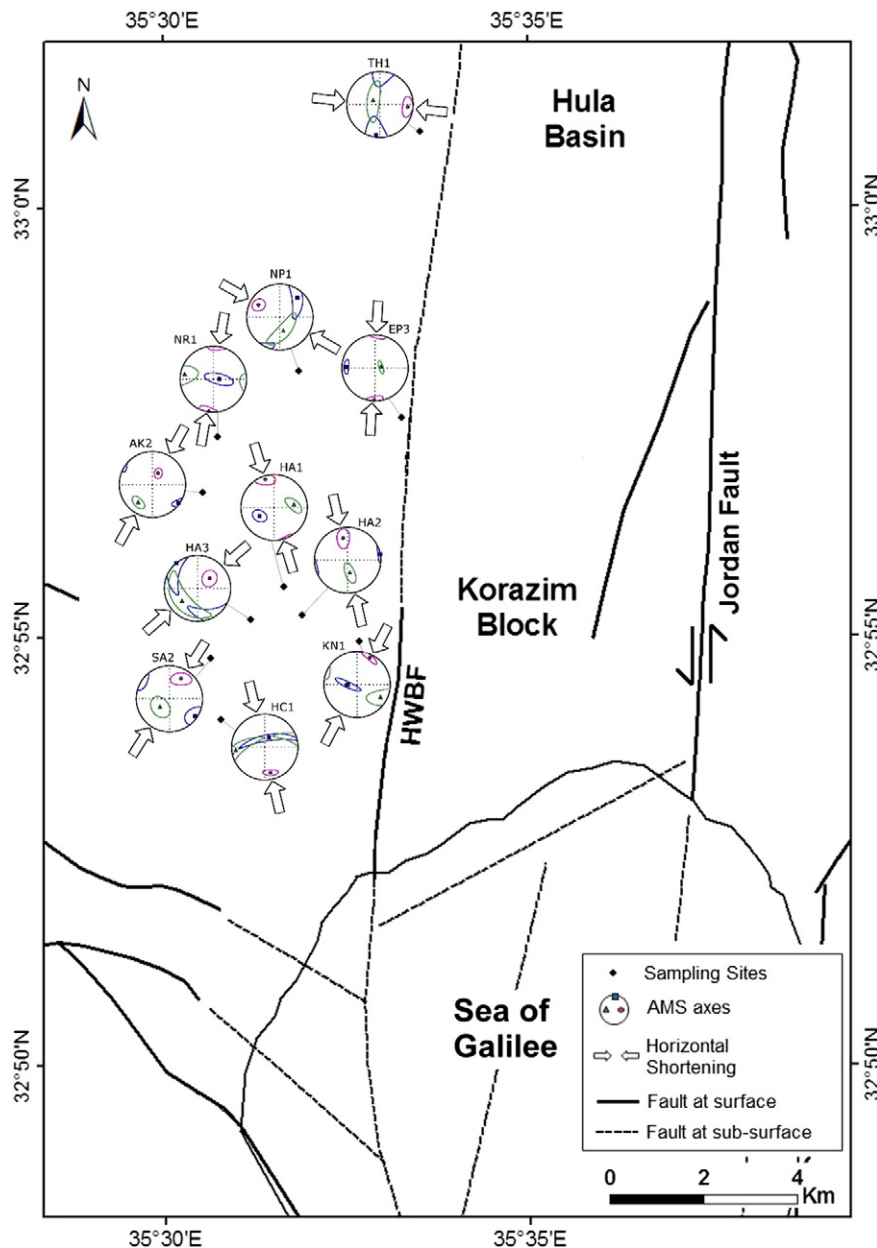


Fig. 9. Map of the main fault segments of the DSF in northern Israel and stereograms of AMS principal axes. Arrows mark the inferred horizontal shortening direction at the sites.

formation of these fractures to a phase of deformation during the late Pleistocene based on U–Th ages of the calcite precipitates. These ~N–S striking calcite-filled fractures are compatible with the AMS-based ~N–S maximum shortening, suggesting that this local strain field conforms with the late Pleistocene deformation.

The deflection of stress/strain trajectories toward major faults can be explained by a number of mechanisms including the (1) effect of “fault strength” or “weak fault” during constant plate motion (Garfunkel, 1981; Zoback et al., 1987), (2) change in the fault geometry (e.g., Saucier et al., 1992), (3) stress/strain buildup at faults tips (e.g., Simón et al., 1999), and (4) stress/strain perturbations during seismic events (e.g., Healy et al., 2004; Nuchter and Ellis, 2011; Nüchter and Stöckhert, 2008; Trepmann and Stöckhert, 2001).

Several indications suggest that mechanisms (2)–(3) are less important. The HWBF is parallel to the ~N–S-striking DSF and shows no indication for geometry change (Fig. 9). The HWBF is ~40 km long, connecting the northwestern edge of the Hula Valley with the Sea of Galilee, probably continues further south under the lake bottom (Sneh and Weinberger, 2014; Fig. 9). Thus, the Rosh Pinna area apparently is located along the fault and not near its tip. At this stage of the study, it is difficult to determine if mechanism (4) has any effect on the deflection process, mainly because the Pleistocene seismicity of the HWBF is not well known and mechanisms (1) and (4) could be mutually connected, e.g., the “fault strength” mechanism might be closely related to dynamic stress perturbation during seismic events. Despite this difficulty, if we consider the possibility that the activity shifted eastward toward the Jordan fault at the end of the Pliocene (Hurwitz et al., 2002), it is possible that dynamic stress perturbation next to the HWBF has not played a major role in deflecting the stress trajectories in the Rosh Pinna area.

The “weak fault” mechanism implies that the stress directions rotate near the HWBF, reducing the shear stress on the main fault. Fault-normal compression (associated with transpression) or fault-parallel tension (associated with transtension) would result in stress trajectories perpendicular or parallel to the fault, respectively, depending on whether the relative plate motion between Sinai and Arabia was convergent or divergent (Garfunkel, 1981). The fault-normal (Metulla block; Levi and Weinberger, 2011) and the fault-parallel (Rosh Pinna area, current study) maximum shortening suggest that the strength of the DSF and variations in plate motion play an important role in deflecting the stress/strain trajectories next to the HWBF.

Garfunkel (1981) suggested that the directions of maximum compression adjacent to the DSF are reoriented toward the fault trace. He noted that this process is dominant mainly close to “free boundaries” such as pull-apart basins and extensional zones. Hence, the trajectories of maximum compression are sub-parallel to the fault traces next to extensional basins and sub-orthogonal next to contraction structures. In the Metulla block, the Garfunkel’s stress trajectories are trending ~W–E, as later confirmed by meso-structures (Weinberger et al., 2009) and AMS analyses (Levi and Weinberger, 2011). In the Rosh Pinna area, the Garfunkel’s stress trajectories are trending ~N–S, as shown by meso-structures (Ron and Eyal, 1985) and the current AMS-based strain analysis.

The effect of the “fault strength” on the stress/strain deflection in the Rosh Pinna area is corroborated in two ways. First, the structural analysis by Weinberger et al. (2009) of the Metulla block suggests that the fault-normal maximum shortening next to the Qiryat Shemona master fault (i.e., the northward continuation of the HWBF) is a consequence of transition from an early (Miocene–Pliocene) phase of pure strike-slip along “strong” DSF to a late (Pleistocene to Recent) phase of convergent strike-slip and strain partitioning along “weak” DSF. Hence, the divergent strike-slip is expected somewhere south of the Metulla block, imposing transtension in the Rosh Pinna area. Second, we consider the fault strength model of Zoback et al. (1987) and Ben-Avraham and Zoback (1992) together with a remote maximum

compression of 340° (Eyal, 1996), N–S striking HWBF and relatively low fault strength. For these conditions, the model predicts that the local maximum compression would deflect and be parallel to the HWBF, imposing transtension in the Rosh Pinna area. Coevally, in the Metulla block, the angle between the remote maximum compression (340°) and the direction of the nearby NNE-striking Yammunneh master fault is about 45°. This might lead to fault-normal maximum compression and transpression in the Metulla block, as long as the Yammunneh fault is weak.

Based on the aforementioned analysis, the AMS-based strain field of ~N–S maximum shortening and ~W–E maximum elongation in the Rosh Pinna area is local and directly associated with the presence of the HWBF. The deflection of the remote stress/strain field near the <10 km sector of the DSF compatibles with the “weakness” of the DSF in northern Israel. Given the history of the geological structures of the area, we suggest that the Rosh Pinna area was under dominant transtension during the Pleistocene. However, the possibility that the transtension began at an earlier stage cannot yet be ruled out and should be considered in the future.

7. Conclusions

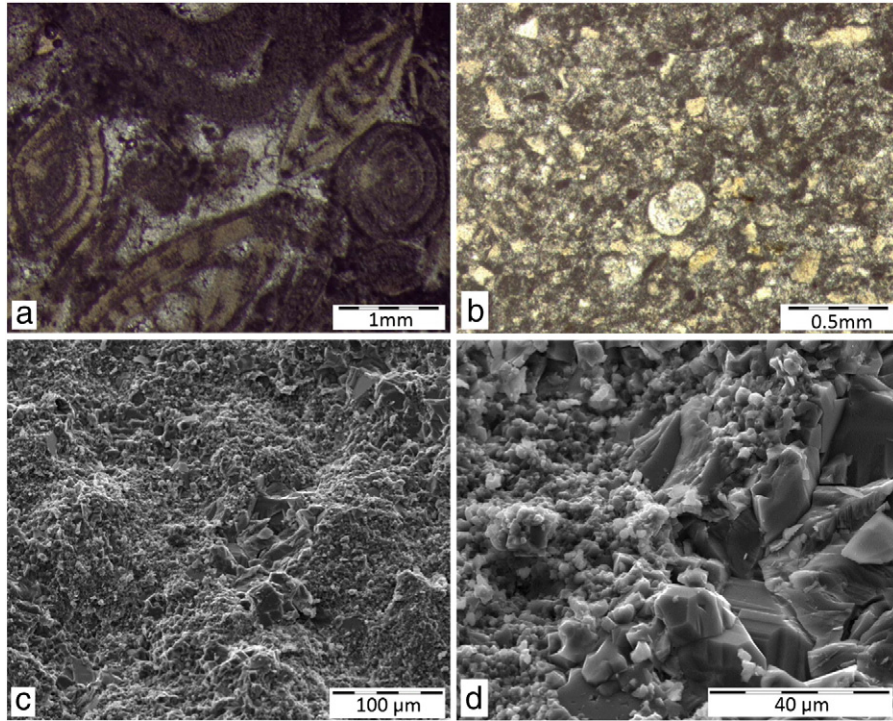
The mean susceptibility, $k_m = -10.67 \pm 1.69 \times 10^{-6}$ SI and the low iron content in the rocks (<300 ppm) show that the Bar-Kokhba limestones from the Rosh-Pinna area are diamagnetic and consisting of almost pure calcite. This indicates that the magnetic fabrics are solely controlled by PCO with k_3 parallel to the calcite c -axes. By separating the diamagnetic sub-fabric in iron-rich carbonate rocks we show that in rocks consisting Fe <500 ppm, the diamagnetic phase controls the AMS. Moreover, the separated diamagnetic sub-fabric supports the conclusion that differences in the anisotropy parameters are related to differences in the strain magnitudes. The spatial distribution of the magnetic fabrics and AMS parameters indicate that strain magnitudes increase eastward with the proximity to the Hula Western Border fault, a main strand of the DSF system in northern Israel. Hence, changes in the AMS parameters recorded by the diamagnetic carbonate rocks are related to spatial and temporal variations in the strain magnitudes.

The majority (80%) of the magnetic fabrics in the Rosh-Pinna area are of tectonic origin, suggesting that the original fabrics were obliterated due to increasing strain. The orientations of k_3 and k_1 axes indicate ~N–S maximum shortening and ~W–E maximum elongation parallel and perpendicular to the strike of the HWBF, respectively. Hence, the remote NNW–SSE maximum shortening (Eyal, 1996) is locally deflected as a consequence of the DSF activity. In light of the “weak fault” model and given the history of the geological structures, we suggest that the study area accommodates transtension during the Pleistocene.

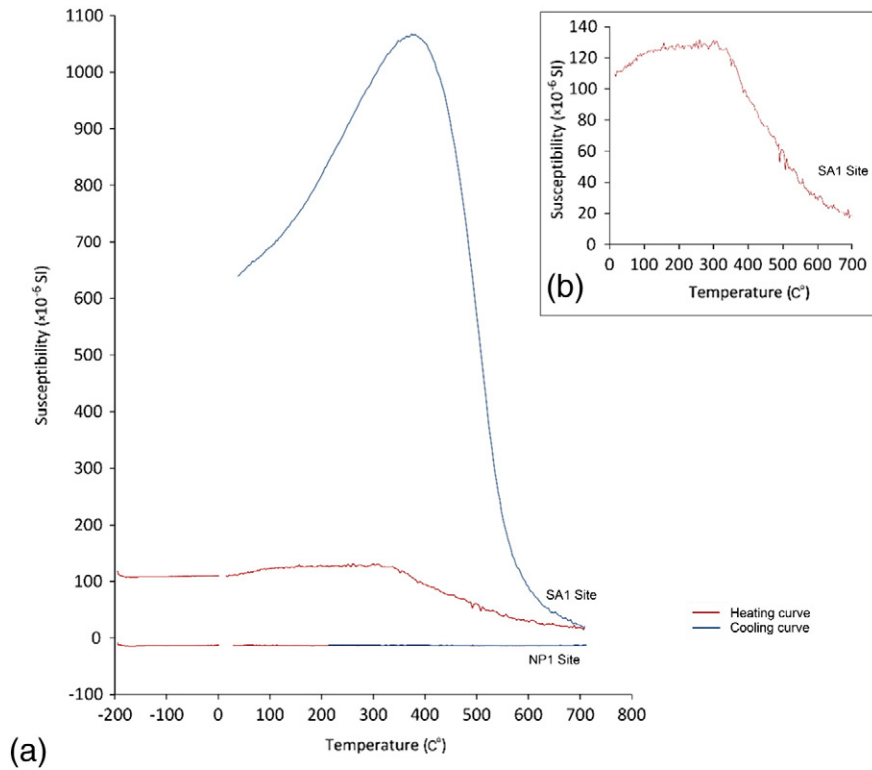
Acknowledgment

This study was supported by grants from the Israel Foundation grant no. 5411245/11 to RW, ISF grant no. 1436/14 to SM, and the Israeli Ministry of National Infrastructures, Energy and Water Resources. We are indebted to Bjarne Almqvist and an anonymous reviewer for thorough and helpful reviews that significantly improved this paper. We are grateful to Yehudit Harlavan for supportive discussion and help in analyzing the geochemical data. We are grateful to Yael Ebert for performing the IRM measurements, and Yehuda Eyal, Meir Abelson and Dafna Brown, for helpful discussions. We would like to thank Graham Borradaile and Mike Jackson for personal consultations. All the data used for this study is accessible at the library of the Geological survey of Israel and online at <http://www.tau.ac.il/~ranissac>

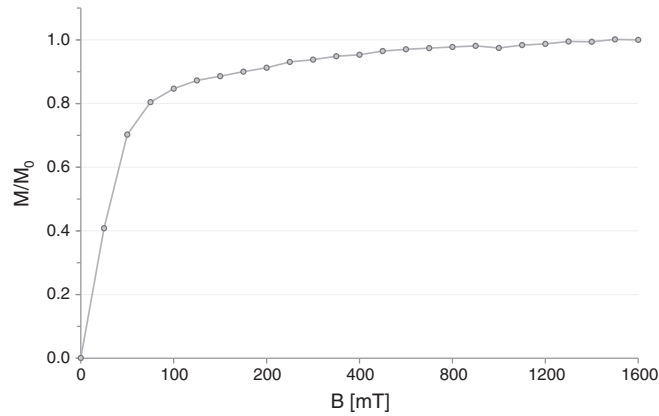
Appendix A



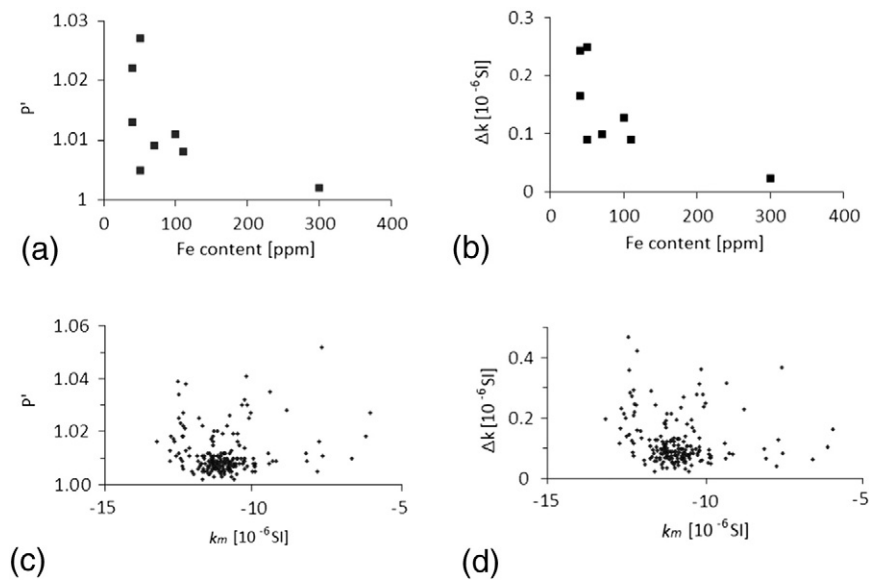
Appendix Fig. A.1. Optical microscopy and SEM images of samples taken from the Eocene Bar-Kokhba Formation limestone. (a) Optical microscopy image of thin-section of sample MG1, showing that the rock is composed of whole Nummulite and foraminifera shells. The shell pores and contact spaces are filled with cement. (b) Optical microscopy image of thin-section of sample KN1, showing uniform matrix composed of fragments of marine shells, interpreted as a result of transportation and sliding events during diagenesis. (c, d) SEM images of sample NP1. The images show homogenous calcite crystalline texture.



Appendix Fig. B.1. (a) Low and high thermomagnetic curves of samples from SA1 and NP1 sites. The low temperatures curves are measured between -200° and 0° and the high temperatures curves are measured between room temperature to 700° . Red and blue lines mark the heating and cooling respectively. (b) Enlargement of the heating curve of sample from SA1 site. SA1 sample shows decrease between 320° and 700° on heating, the susceptibility drops by 80%. This may suggest the existence of ferromagnetic minerals, maybe even iron sulfides as its typical Curie temperature is around $\sim 320^{\circ}$ (Hunt et al., 1995). The cooling curve indicates irreversibility with great increase until $\sim 380^{\circ}$ suggesting the creation of new magnetic minerals.



Appendix Fig. C.1. IRM of sample from SA1 site. Saturation below 200 [mT] associated with magnetite grains. After saturation of the soft (ferromagnetic) minerals the curve continues moderately to increase indicating high coercivity minerals.



Appendix Fig. D.1. Samples of the Bar-Kokhba limestones: (a) Corrected anisotropy degree versus Fe content ($N = 8$). (b) Susceptibility difference versus Fe content ($N = 8$). (c) Corrected anisotropy degree versus mean susceptibility ($N = 193$). (d) Susceptibility difference versus mean susceptibility ($N = 193$).

References

- Almqvist, B.S.G., Hirt, A.M., Schmidt, V., Dietrich, D., 2009. Magnetic fabrics of the Morcles Nappe complex. *Tectonophysics* 466 (1–2), 89–100. <http://dx.doi.org/10.1016/j.tecto.2008.07.014>.
- Almqvist, B.S.G., Herwegh, M., Schmidt, V., Pettke, T., Hirt, A.M., 2010. Magnetic susceptibility as a tool to study deformed calcite with variable impurity content. *Geochem. Geophys. Geosyst.* 11. <http://dx.doi.org/10.1029/2009gc002900> (Q01z09).
- Almqvist, B.S.G., Hirt, A.M., Herwegh, M., Leiss, B., 2011. Magnetic anisotropy reveals Neogene tectonic overprint in highly strained carbonate mylonites from the Morcles nappe, Switzerland. *J. Struct. Geol.* 33 (5), 1010–1022.
- Arkin, Y., 1996. Fractures and karst in hard carbonates in northern Israel. *Geol. Surv. Curr. Res.* 10 (90).
- Arkin, Y., Kagan, E., Matthews, M.B., Ayalon, A., Ram, E., 2004. IGS Meeting, March 2004: for more details, please find in the GSI library.
- Balsley, J.R., Buddington, A.F., 1960. Magnetic susceptibility anisotropy and fabric of some Adirondack granites and orthogneisses. *Am. J. Sci.* 258, 6–20.
- Bartov, Y., Steinitz, G., Eyal, M., Eyal, Y., 1980. Sinistral movement along the Gulf of Aqaba—its age and relation to the opening of the Red Sea. *Nature* 285, 220–221.
- Ben-Avraham, Z., Zoback, M.D., 1992. Transform-normal extension and asymmetric basins—an alternative to pull-apart models. *Geology* 20 (5), 423–426.
- Bestmann, M., Kunze, K., Matthews, A., 2000. Evolution of a calcite marble shear zone complex on Thassos Island, Greece: microstructural and textural fabrics and their kinematic significance. *J. Struct. Geol.* 22 (11), 1789–1807.
- Bishop, J.F.W., 1953. A theoretical examination of the plastic deformation of crystals by glide. *Philos. Mag. Ser. 7* 44 (348), 51–64. <http://dx.doi.org/10.1080/14786440108520274>.
- Bishop, J.F.W., Hill, R., 1951. A theory of the plastic distortion of a polycrystalline aggregate under combined stresses. *Philos. Mag. Ser. 7* 42 (327), 414–427. <http://dx.doi.org/10.1080/14786445108561065>.
- Bogoch, R., Sneh, A., 2008. *Geological Map of Israel. Sheet 4-I, Arbel, scale 1:50,000.*
- Borradaile, G., 1987. Anisotropy of magnetic-susceptibility—rock composition versus strain. *Tectonophysics* 138 (2–4), 327–329. [http://dx.doi.org/10.1016/0040-1951\(87\)90051-5](http://dx.doi.org/10.1016/0040-1951(87)90051-5).
- Borradaile, G.J., 1988. Magnetic-susceptibility, petrofabrics and strain. *Tectonophysics* 156 (1–2), 1–20. [http://dx.doi.org/10.1016/0040-1951\(88\)90279-x](http://dx.doi.org/10.1016/0040-1951(88)90279-x).
- Borradaile, G.J., 1991. Correlation of strain with anisotropy of magnetic-susceptibility (AMS). *Pure Appl. Geophys.* 135 (1), 15–29. <http://dx.doi.org/10.1007/bf00877006>.
- Borradaile, G.J., Hamilton, T., 2004. Magnetic fabrics may proxy as neotectonic stress trajectories, Polis rift, Cyprus. *Tectonics* 23 (1). <http://dx.doi.org/10.1029/2002TC001434> (n/a–n/a).
- Borradaile, G.J., Henry, B., 1997. Tectonic applications of magnetic susceptibility and its anisotropy. *Earth Sci. Rev.* 42 (1–2), 49–93.
- Borradaile, G.J., Jackson, M., 2004. Anisotropy of magnetic susceptibility (AMS): magnetic petrofabrics of deformed rocks. *Geol. Soc. Lond., Spec. Publ.* 238, 299–360.
- Borradaile, G.J., Jackson, M., 2010. Structural geology, petrofabrics and magnetic fabrics (AMS, AARM, AIRM). *J. Struct. Geol.* 32 (10), 1519–1551. <http://dx.doi.org/10.1016/j.jsg.2009.09.006>.
- Borradaile, G.J., Lagroix, F., Hamilton, T.D., Trebilcock, D.A., 2010. Ophiolite tectonics, rock magnetism and palaeomagnetism, Cyprus. *Surv. Geophys.* 31 (3), 285–359. <http://dx.doi.org/10.1007/s10712-009-9090-2>.
- Braun, D., Weinberger, R., Eyal, Y., Feinstein, S., Harlavan, Y., Levi, T., 2015. Distinctive diamagnetic fabrics in dolostones evolved at fault cores, the Dead Sea Transform. *J. Struct. Geol.* 77, 11–26. <http://dx.doi.org/10.1016/j.jsg.2015.05.007>.
- Calnan, E.A., Clews, C.J.B., 1950. Deformation textures in face-centred cubic metals. *Philos. Mag. Ser. 7* 41 (322), 1085–1100. <http://dx.doi.org/10.1080/14786445008561151>.

- Calnan, E.A., Clews, C.J.B., 1951. The development of deformation textures in metals: Part II. Body-centred cubic metals. *Philos. Mag. Ser. 7* 42 (329), 616–635. <http://dx.doi.org/10.1080/14786445108561277>.
- Chadima, H.A., Hirt, A., Hrouda, F., Heinrich, S.M., 2004. Phyllosilicate preferred orientation as a control of magnetic fabric: evidence from neutron texture goniometry and low and high-field magnetic anisotropy (SE Rhenohercynian Zone of Bohemian Massif). *Geol. Soc. Lond.* 238, 361–380.
- Cogne, J.P., Perroud, H., 1988. Anisotropy of magnetic-susceptibility as a strain-gauge in the flamanville granite, NW France. *Phys. Earth Planet. Inter.* 51 (4), 264–270. [http://dx.doi.org/10.1016/0031-9201\(88\)90068-4](http://dx.doi.org/10.1016/0031-9201(88)90068-4).
- Cullity, B.D., 1972. *Introduction to Magnetic Materials*. ADDISON-WESLEY, University of Notre Dame.
- De Wall, H., Bestmann, M., Ullemeyer, K., 2000. Anisotropy of diamagnetic susceptibility in Thassos marble: a comparison between measured and modeled data. *J. Struct. Geol.* 22 (11–12), 1761–1771. [http://dx.doi.org/10.1016/S0191-8141\(00\)00105-x](http://dx.doi.org/10.1016/S0191-8141(00)00105-x).
- Dietrich, D., Song, H., 1984. Calcite fabric in a natural shear environment, the helvetic nappes of western Switzerland. *J. Struct. Geol.* 6 (1–2), 19–32. [http://dx.doi.org/10.1016/0191-8141\(84\)90080-4](http://dx.doi.org/10.1016/0191-8141(84)90080-4).
- Evans, M., Lewchuk, M., Elmore, R., 2003. Strain partitioning of deformation mechanisms in limestones: examining the relationship of strain and anisotropy of magnetic susceptibility (AMS). *J. Struct. Geol.* 25 (9), 1525–1549. [http://dx.doi.org/10.1016/S0191-8141\(02\)00186-4](http://dx.doi.org/10.1016/S0191-8141(02)00186-4).
- Eyal, Y., 1996. Stress field fluctuations along the Dead Sea rift since the middle Miocene. *Tectonics* 15 (1), 157–170.
- Eyal, Y., Reches, Z., 1983. Tectonic analysis of the Dead Sea rift region since the Late-Cretaceous based on mesostructures. *Tectonics* 2 (2), 39–66.
- Freund, R., Garfunkel, Z., Zak, I., Goldberg, M., Weissbrod, T., Derin, B., 1970. The shear along the Dead Sea rift. *Phil. Trans. R. Soc. London A* 267, 107–130.
- Fuller, M., Cisowski, S., Hart, M., Haston, R., Schmidtke, E., Jarrard, R., 1988. NRM-IRM(S) demagnetization plots - an aid to the interpretation of natural remanent magnetization. *Geophys. Res. Lett.* 15 (5), 518–521. <http://dx.doi.org/10.1029/G10151005p00518>.
- Garfunkel, Z., 1981. Internal structure of the Dead Sea leaky transform (rift) in relation to plate kinematics. *Tectonophysics* 80, 81–108.
- Hamilton, T.D., Borradaile, G.J., Lagroix, F., 2004. Sub-fabric identification by standardization of AMS: an example of inferred neotectonic structures from Cyprus. *Geol. Soc. Lond., Spec. Publ.* 238, 527–540.
- Healy, D., Yielding, G., Kuszniir, N., 2004. Fracture prediction for the 1980 El Asnam, Algeria earthquake via elastic dislocation modeling. *Tectonics* 23 (6). <http://dx.doi.org/10.1029/2003TC001575> (n/a–n/a).
- Heimann, A., Ron, H., 1993. Geometric changes of plate boundaries along part of the northern Dead Sea Transform: geochronologic and paleomagnetic evidence. *Tectonics* 12 (2), 477–491.
- Henry, B., Daly, L., 1983. From qualitative to quantitative magnetic-anisotropy analysis - the prospect of finite strain calibration. *Tectonophysics* 98 (3–4), 327–336. [http://dx.doi.org/10.1016/0040-1951\(83\)90300-1](http://dx.doi.org/10.1016/0040-1951(83)90300-1).
- Hirt, A.M., Lowrie, W., Clendenen, W.S., Kligfield, R., 1988. The correlation of magnetic-anisotropy with strain in the chelmsford formation of the sudbury basin, Ontario. *Tectonophysics* 145 (3–4), 177–189. [http://dx.doi.org/10.1016/0040-1951\(88\)90194-1](http://dx.doi.org/10.1016/0040-1951(88)90194-1).
- Hobbs, B.E., Means, W.D., Williams, P.F., 1976. *An Outline of Structural Geology*. Wiley.
- Hounslow, M.W., 2001. The crystallographic fabric and texture of siderite in concretions: implications for siderite nucleation and growth processes. *Sedimentology* 48.
- Hrouda, F., Henry, B., Borradaile, G., 2000. Limitations of tensor subtraction in isolating diamagnetic fabrics by magnetic anisotropy. *Tectonophysics* 322 (3–4), 303–310. [http://dx.doi.org/10.1016/S0040-1951\(00\)00093-7](http://dx.doi.org/10.1016/S0040-1951(00)00093-7).
- Hrouda, F., 2004. Problems in interpreting AMS parameters in diamagnetic rocks. *Geol. Soc. Lond., Spec. Publ.* 238, 49–59 (2004).
- Hrouda, F., Krejci, O., Potfaj, M., Stranik, Z., 2009. Magnetic fabric and weak deformation in sandstones of accretionary prisms of the Flysch and Klippen Belts of the Western Carpathians: mostly offscraping indicated. *Tectonophysics* 479 (3–4), 254–270. <http://dx.doi.org/10.1016/j.tecto.2009.08.016>.
- Hunt, C.P., Moskowitz, B.M., Banerjee, S.K., 1995. Magnetic properties of rocks and minerals. In: Ahrens, T.J. (Ed.), *Rock physics & phase relations: a handbook of physical constants*. 3, pp. 189–204. <http://dx.doi.org/10.1029/RF003>.
- Hurwitz, S., Garfunkel, Z., Ben-Gai, Y., Reznikov, M., Rotstein, Y., Gvirtzman, H., 2002. The tectonic framework of a complex pull-apart basin: seismic reflection observations in the Sea of Galilee, Dead Sea transform. *Tectonophysics* 359 (3–4), 289–306. [http://dx.doi.org/10.1016/S0040-1951\(02\)00516-4](http://dx.doi.org/10.1016/S0040-1951(02)00516-4).
- Jackson, M., 1991. Anisotropy of magnetic remanence: a brief review of mineralogical sources, physical origins, and geological applications, and comparison with susceptibility anisotropy. *Pure Appl. Geophys.* 136 (1), 1–28. <http://dx.doi.org/10.1007/bf00878885>.
- Jackson, M., Tauxe, L., 1991. Anisotropy of magnetic-susceptibility and remanence-developments in the characterization of tectonic, sedimentary and igneous fabric. *Rev. Geophys.* 29, 371–376.
- Jayangondaperumal, R., Dubey, A.K., Kumar, B.S., Wesnosky, S.G., Sangode, S.J., 2010. Magnetic fabrics indicating Late Quaternary seismicity in the Himalayan foothills. *Int. J. Earth Sci.* 99, S265–S278. <http://dx.doi.org/10.1007/s00531-009-0494-5>.
- Jelinek, V., 1977. *The Statistical Theory of Measuring Anisotropy of Magnetic Susceptibility of Rocks and Its Application*. G. Brno (Ed.).
- Jelinek, V., 1981. Characterization of the magnetic fabric of rocks. *Tectonophysics* 79 (3–4), T63–T67. [http://dx.doi.org/10.1016/0040-1951\(81\)90110-4](http://dx.doi.org/10.1016/0040-1951(81)90110-4).
- Kamb, W.B., 1959. Theory of preferred crystallographic orientation developed under stress. *J. Geol.* 67, 153–160.
- Kligfield, W., Pfiffner, O.A., Lowrie, R.W., 1982. Magnetic properties of deformed oolitic limestones from the Swiss Alps: the correlation of magnetic anisotropy and strain. *Ecol. Geol. Helv.* 75 (0012-9402).
- Latta, D.K., Anastasio, D.J., 2007. Multiple scales of mechanical stratification and decollement fold kinematics, Sierra Madre Oriental foreland, northeast Mexico. *J. Struct. Geol.* 29 (7), 1241–1255. <http://dx.doi.org/10.1016/j.jsg.2007.03.012>.
- Levi, T., Weinberger, R., 2011. Magnetic fabrics of diamagnetic rocks and the strain field associated with the Dead Sea Fault, northern Israel. *J. Struct. Geol.* 33 (4), 566–578. <http://dx.doi.org/10.1016/j.jsg.2011.02.001>.
- Levitte, D., 2001. *Geological Map of Israel. Sheet 2-III, Zefat, scale 1:50,000*.
- Mamtani, M.A., Sengupta, A., 2009. Anisotropy of magnetic susceptibility analysis of deformed kaolinite: implications for evaluating landslides. *Int. J. Earth Sci.* 98 (7), 1721–1725. <http://dx.doi.org/10.1007/s00531-008-0336-x>.
- Martin-Hernandez, F., Ferre, E.C., 2007. Separation of paramagnetic and ferrimagnetic anisotropies: a review. *J. Geophys. Res. Solid Earth* 112 (B3). <http://dx.doi.org/10.1029/2006jb004340> (B03105).
- McKenzie, D.R., Yin, Y., McFall, W.D., Hoang, N.H., 1996. The orientation dependence of elastic strain energy in cubic crystals and its application to the preferred orientation in titanium nitride thin films. *J. Phys. Condens. Matter* 8 (32), 5883–5890. <http://dx.doi.org/10.1088/0953-8984/8/32/008>.
- Mullins, C.E., 1977. Magnetic-susceptibility of soil and its significance in soil science—review. *J. Soil Sci.* 28 (2), 223–246.
- Nagata, T., 1961. *Chemical Remanent Magnetization*. In: Nagata, T. (Ed.), *Rock Magnetism*. Maruzen Co. LTD, Tokyo, p. 350.
- Neumann, E., 1969. Experimental recrystallisation of dolomite and comparison of preferred orientations of calcite and dolomite in deformed rocks. *J. Geol.* 77, 426–438.
- Nuchter, J.A., Ellis, S., 2011. Mid-crustal controls on episodic stress-field rotation around major reverse, normal and strike-slip faults. *Geol. Soc. Lond., Spec. Publ.* 359 (1), 187–201. <http://dx.doi.org/10.1144/SP359.11>.
- Nüchter, J.A., Stöckert, B., 2008. Coupled stress and pore fluid pressure changes in the middle crust: vein record of coseismic loading and postseismic stress relaxation. *Tectonics* 27 (1). <http://dx.doi.org/10.1029/2007TC002180> (n/a–n/a).
- Nye, J.F., 1957. *Physical Properties of Crystals: Their Representation by Tensors And Matrices*. O. S. Publications (Ed.).
- Owens, W.H., Bamford, D., 1976. Magnetic, seismic, and other anisotropic properties of rock fabrics. *Philos. Trans. R. Soc. Lond. A Math. Phys. Eng. Sci.* 283 (1312), 55–68. <http://dx.doi.org/10.1098/rsta.1976.0069>.
- Owens, W.H., Rutter, E.H., 1978. The development of magnetic susceptibility anisotropy through crystallographic preferred orientation in a calcite rock. *Phys. Earth Planet. Inter.* 16 (3), 215–222.
- Parés, J.M., van der Pluijm, B., 2004. Correlating magnetic fabrics with finite strain: comparing results from mudrocks in the Variscan and Appalachian Orogens. *Geol. Acta* 2 (3).
- Parés, J.M., van der Pluijm, B.A., Dinares-Turell, J., 1999. Evolution of magnetic fabrics during incipient deformation of mudrocks (Pyrenees, northern Spain). *Tectonophysics* 307 (1–2), 1–14.
- Patterson, M.S., 1973. Nonhydrostatic thermodynamics and its geologic application. *Rev. Geophys.* 11, 355–389.
- Quennell, A.M., 1959. *Tectonics of the Dead Sea rift*. Congreso Geológico Internacional, 20th session, Asociación de Servicios Geológicos Africanos, Mexico City, pp. 385–405.
- Ron, H., Eyal, Y., 1985. Intraplate deformation by block rotation and mesostructures along the Dead Sea transform. *Tectonics* 4, 85–105.
- Rotstein, Y., Bartov, Y., 1989. Seismic reflection across a continental transform: an example from a convergent segment of the Dead Sea rift. *J. Geophys. Res.* 94, 2902–2912.
- Rutter, E.H., Rusbridge, M., 1977. The effect of non-coaxial strain paths on crystallographic preferred orientation development in the experimental deformation of a marble. *Tectonophysics* 39 (1–3), 73–86.
- Rutter, E.H., Casey, M., Burlini, L., 1994. Preferred crystallographic orientation development during the plastic and superplastic flow of calcite rocks. *J. Struct. Geol.* 16 (10), 1431–1446. [http://dx.doi.org/10.1016/0191-8141\(94\)90007-8](http://dx.doi.org/10.1016/0191-8141(94)90007-8).
- Saucier, F., Humphreys, E., Weldon, R., 1992. Stress near geometrically complex strike-slip faults: application to the San Andreas Fault at Cajon Pass, southern California. *J. Geophys. Res.* 97 (B4), 5081. <http://dx.doi.org/10.1029/91JB02644>.
- Schmidt, V., Gunther, D., Hirt, A.M., 2006. Magnetic anisotropy of calcite at room-temperature. *Tectonophysics* 418 (1–2), 63–73. <http://dx.doi.org/10.1016/j.tecto.2005.12.019>.
- Schmidt, V., Hirt, A.M., Rosselli, P., Martin-Hernandez, F., 2007. Separation of diamagnetic and paramagnetic anisotropy by high-field, low-temperature torque measurements. *Geophys. J. Int.* 168 (1), 40–47. <http://dx.doi.org/10.1111/j.1365-246X.2006.03202.x>.
- Schmidt, V., Hirt, A.M., Leiss, B., Burlini, L., Walter, J.M., 2009. Quantitative correlation of texture and magnetic anisotropy of compacted calcite-muscovite aggregates. *J. Struct. Geol.* 31 (10), 1062–1073. <http://dx.doi.org/10.1016/j.jsg.2008.11.012>.
- Siegesmund, S., Ullemeyer, K., Dahms, M., 1995. Control of magnetic rock fabrics by mica preferred orientation—a quantitative approach. *J. Struct. Geol.* 17 (11), 1601. [http://dx.doi.org/10.1016/0191-8141\(95\)00047-h](http://dx.doi.org/10.1016/0191-8141(95)00047-h).
- Simón, J.L., Arlegui, L.E., Liesa, C.L., Maestro, A., 1999. Stress perturbations registered by jointing near strike-slip, normal, and reverse faults: examples from the Ebro Basin, Spain. *J. Geophys. Res.* 104 (B7), 15141. <http://dx.doi.org/10.1029/1998JB900070>.
- Sneh, A., Weinberger, R., 2006. *Geological Map of Israel. Sheet 2-IV, Rosh Pinna, scale 1:50,000*.
- Sneh, A., Weinberger, R., 2014. *Major Structures of Israel and Environs, scale 1:500,000*.
- Soto, R., Casas-Sainz, A.M., Villalain, J.J., Oliva-Urcia, B., 2007. Mesozoic extension in the Basque-Cantabrian basin (N Spain): contributions from AMS and brittle

- mesostructures. *Tectonophysics* 445 (3–4), 373–394. <http://dx.doi.org/10.1016/j.tecto.2007.09.007>.
- Soto, R., Larrasoana, J.C., Arlegui, L.E., Beamud, E., Oliva-Urcia, B., Simon, J.L., 2009. Reliability of magnetic fabric of weakly deformed mudrocks as a palaeostress indicator in compressive settings. *J. Struct. Geol.* 31 (5), 512–522. <http://dx.doi.org/10.1016/j.jsg.2009.03.006>.
- Stacey, F.D., Joplin, G., Lindsay, J., 1960. Magnetic anisotropy and fabric of some foliated rocks from S.E. Australia. *Geofisica Pura E Applicata* 47 (1), 30–40. <http://dx.doi.org/10.1007/BF01992481>.
- Stockhausen, H., 1998. Some new aspects for the modelling of isothermal remanent magnetization acquisition curves by cumulative log Gaussian functions. *Geophys. Res. Lett.* 25 (12), 2217–2220. <http://dx.doi.org/10.1029/98gl01580>.
- Tarling, D.H., Hrouda, F.H., 1993. *The Magnetic Anisotropy of Rocks*. Chapman and Hall, London.
- Trepmann, C., Stöckhert, B., 2001. Mechanical twinning of jadeite—an indication of synseismic loading beneath the brittle–plastic transition. *Int. J. Earth Sci.* 90 (1), 4–13. <http://dx.doi.org/10.1007/s005310000165>.
- Tripathy, N.R., Srivastava, H.B., Mamtani, M.A., 2009. Evaluation of a regional strain gradient in mylonitic quartzites from the footwall of the Main Central Thrust Zone (Garhwal Himalaya, India): inferences from finite strain and AMS analyses. *J. Asian Earth Sci.* 34 (1), 26–37. <http://dx.doi.org/10.1016/j.jseae.2008.03.008>.
- Tullis, J., Yund, R.A., 1982. Grain growth kinetics of quartz and calcite aggregates. *J. Geol.* 90, 308–318.
- Weinberger, R., Gross, M.R., Sneh, A., 2009. Evolving deformation along a transform plate boundary: Example from the Dead Sea Fault in northern Israel. *Tectonics* 28.
- Wenk, H.R., Takeshita, T., Bechler, E., Erskine, B.G., Matthies, S., 1987. Pure shear and simple shear calcite textures—comparison of experimental, theoretical and natural data. *J. Struct. Geol.* 9 (5–6), 731–745. [http://dx.doi.org/10.1016/0191-8141\(87\)90156-8](http://dx.doi.org/10.1016/0191-8141(87)90156-8).
- Zoback, M.D., Zoback, M.L., Mount, V.S., Suppe, J., Eaton, J.P., Healy, J.H., Oppenheimer, D., Reasenber, P., Jones, L., Raleigh, C.B., Wong, I.G., Scotti, O., Wentworth, C., 1987. New evidence on the state of stress of the San Andreas fault system. *Science* 238, 1105–1111.